HTD-Vol.363/BED-Vol.44
Advances in Heat and Mass Transfer in Biotechnology – 1999
ASME 1999

TEMPERATURE DEPENDENT TISSUE PROPERTIES AND ULTRASONIC LESION FORMATION

Michael C. Kolios[1]
Department of Mathematics,
Physics and Computer Science,
Ryerson Polytechnic University,
Toronto, Ontario, M5B-2K3,
Canada
mkolios@acs.ryerson.ca

Michael D. Sherar

Department of Medical Biophysics,
University of Toronto,
Toronto, Ontario, M5G-2M9,
Canada
sherar@oci.utoronto.ca

John W. Hunt

Department of Medical Biophysics,
University of Toronto,
Toronto, Ontario, M5G-2M9,
Canada
hunt@oci.utoronto.ca

ABSTRACT

High intensity focused ultrasound has considerable potential for the noninvasive treatment of localised disease. A detailed understanding of the kinetics of tissue coagulation is required to optimise ultrasonic parameters. In this presentation a theoretical model was used to examine the effects of temperature dependent ultrasonic attenuation and absorption on the transient tissue temperature distributions and lesion dimensions. A finite difference algorithm was used to solve numerically the nonlinear form of the bioheat transfer equation in cylindrical coordinates. The lesion dimensions were calculated based on the time-temperature distributions in tissue by using a thermal dose threshold to define the lesion boundaries. The results were compared to published experimental data in which the the location of maximal energy deposition during short duration high intensity focused ultrasound irradiation of in vitro tissue was examined. It was found that the theoretical model did not predict the size and shape of the experimental lesions. To correctly predict lesion size and shape much higher values of attenuation and absorption were required than can be accounted for by thermal coagulation of the tissue alone. The values used suggest that for intensities greater than 3030 W/cm^2 the effective local attenuation/absorption in the focal region increased by a factor of 10-20. It is finally shown that temperature dependent tissue changes should be incorporated in thermal models to avoid underestimation of the induced temperature distributions during high intensity focused ultrasound therapy.

1 Introduction

High intensity focused ultrasound (HIFU) has been used clinically as a non-invasive surgical technique in the fields of opthalmology (Burgess et al. 1986), neurology (Fry and Fry 1960), urology (Sanghvi et al. 1996) and oncology (Vallancien et al. 1996). The tissue in the focal region of the ultrasound beam coagulates and forms a "lesion" destroying the pathological tissue while sparing the surrounding healthy tissue. Treatment optimisation however requires a detailed understanding of the kinetics of lesion formation, particularly for large target volumes that involve multiple sonications. To control the formation of a lesion, it is desirable to avoid very high ultrasonic intensities that produce cavitation since this process is not well understood and produces lesions of unpredictable size (Malcolm and ter Haar 1996). In contrast, lesions produced through purely thermal mechanisms have well defined and reproducible boundaries. In this case tissue temperatures attained during the procedure can be estimated using linear bioheat transfer models (Kolios et al. 1996).

The two most dominant tissue property variations that could potentially effect the temperature distribution *in-vivo* are changes in the tissue ultrasonic attenuation and absorption coefficients and modifications to blood flow in the irradiated region. Recent

[1]Address all correspondence to this author.

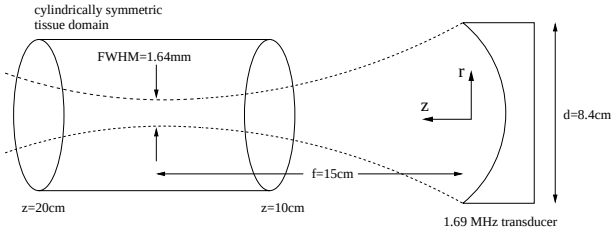

Figure 1. *The simulation geometry. A cylindrically symmetric tissue volume was irradiated by a focused transducer.*

work suggests that the attenuation and absorption coefficients increase as a function of temperature and exposure time (Damianou et al. 1995; Damianou et al. 1997; Gertner et al. 1997; Gertner et al. 1998). This theoretical investigation examines the changes in ultrasonic lesion size due to dynamic variations in the tissue attenuation and absorption during HIFU therapy.

2 Methods

The temperature distribution in the heated tissues was calculated using the Pennes bioheat transfer equation in cylindrical coordinates assuming cylindrical symmetry:

$$\rho_t c_t \frac{\partial T}{\partial t} = k_t\left(\frac{\partial^2 T}{\partial^2 r} + \frac{1}{r}\frac{\partial T}{dr} + \frac{\partial^2 T}{\partial^2 z}\right) - w_b(r,z,t)c_b(T(r,z,t) - T_{art}) + P(r,z,t) \quad (1)$$

where ρ is the density (g/cm^3), c is the specific heat capacity (J/g/^{o}C), T is the temperature (^{o}C), k is the thermal conductivity (W/cm/^{o}C), w is the volumetric perfusion rate (g/cm^3/s) and P is the volumetric power deposition rate (W/cm^3). Subscripts t, b and *art* denote tissue, blood and arterial respectively.

The equation was solved using a finite difference computational model (Kolios et al. 1995). The method described in Patankar (1980) was used to solve the nonlinear form of the equation in which tissue attenuation and absorption were temperature dependent. To accelerate the calculations, a variable grid was used in the radial direction that increased the grid spacing dr_i linearly from 0.001 mm at the origin to a maximum of 0.2 mm at the edge. The axial spacing dz was set to 1 mm and the timestep dt to 0.1 s or 0.01 s, depending on the rate of convergence of the calculations. The computational domain radius was 2 cm (figure 1). This resulted in a mesh of 201 by 101 nodes. The values assigned to the thermal properties used in equation 1 are listed in table 1 and the ultrasonic parameters in table 2. The ambient temperature was set to 21 °C to match the experimental data (which is the boundary condition for all cylinder surfaces).

Table 1. List of thermal parameters used in simulations.

tissue/blood specific heat capacity, c (J/g/°C):	3.55
tissue/blood density, ρ (g/cm^3):	1
tissue/blood conductivity, k (W/cm/°C):	0.005

Table 2. List of ultrasonic parameters used in simulations.

transducer frequency, f (MHz):	1.69
transducer radius of curvature, R (cm):	15
transducer diameter, D (cm):	8.4
intensity attenuation coefficient, η_o (Np/cm):	0.084
intensity attenuation coefficient, η_l (lesioned tissue) (Np/cm):	0.176
intensity absorption coefficient, μ (% of η):	90

Lesion dimensions were calculated using a threshold thermal dose to define the boundary between coagulated and normal tissue. A thermal dose can be defined that relates the time (t) required to produce an isoeffect (*e.g.* 3 logs of cell kill) at temperature T to the equivalent time (TD_{43}) which would be required to produce the same effect at 43°C (Sapareto and Dewey 1984):

$$TD_{43} = \sum_{t=t_o}^{t_{end}} 2^{T(t)-43}\Delta t,\ T >= 42.5^oC$$
$$TD_{43} = \sum_{t=t_o}^{t_{end}} 0.5^{T(t)-42.5}\Delta t,\ T < 42.5^\circ C \quad (2)$$

This expression has been shown to hold for experiments with cell survival as the endpoint (for the temperature range of 41-57°C, (Borelli et al. 1990)) and a similar expression *in vivo* with tissue necrosis as the endpoint (for the temperature range of 41-48°C, (Linke et al. 1967)). The threshold used for tissue lesioning (whitening) as the endpoint for the *in-vitro* experiments was TD_{43} = 2x10^8 s.

The ultrasonic intensity distributions were calculated using the method described in Arditi et al. (1981). The transducer focal length f was 15 cm, its diameter was 10 cm (with an active aperture of 8.4 cm) and was operated at 1.69 MHz. The power absorption pattern in the tissues was calculated using:

$$P(r,z,t) = \mu(r,z,t)I(r,z)e^{\int_{z_o}^{z} -\eta(r,z,t)dz} \quad (3)$$

where P is the power absorbed (W/cm^3), μ is the ultrasound absorption coefficient (Np/cm), $I(r,z)$ is the "free-field" intensity profile of the beam (in a water-tank, W/cm^2), η is the ultrasound attenuation coefficient (Np/cm) and z_o is the axial location of the

Table 3. List of general parameters used in simulations.

ex-vivo bladder & liver threshold thermal dose, TD_{43} (s) :	2×10^8
in-vivo liver threshold thermal dose, TD_{43} (s):	3600
thermal dose threshold for onset of attenuation change , TD_{43_o} (s):	6×10^3
thermal dose threshold for end of attenuation change , TD_{43_l} (s):	6×10^8

waterbath/tissue boundary. To simplify and accelerate the calculations, it was assumed that the free-field beam intensity I(r,z) was not significantly distorted by the presence of the tissue and that the attenuated beam can be calculated by integrating the attenuation coefficient over the axial distance traversed. Numerical integration was performed using the integration solver DQNC79 available through the SLATEC library[2]. The routine integrates a function using a 7-point adaptive Newton-Cotes quadrature rule.

The change in attenuation and absorption as a function of thermal dose was modeled according to the experimental data of Damianou et al. (1995). The equation used to model the thermal dose dependence of the ultrasonic attenuation was:

$$\eta(TD_{43}) = \frac{(\eta_l - \eta_o)}{ln(TD_{43_l}) - ln(TD_{43_o})} ln(TD_{43}) + C, \quad 60 \times 10^2 s \leq TD_{43} \leq 60 \times 10^7 s \qquad (4)$$

where the subscript l refers to the tissue properties after which tissue attenuation reaches a plateau and does not increase with increasing thermal dose (lesioned tissue) and o refers to the initial properties before any changes have occurred as a result of tissue heating. C in equation 4 represents a constant of the fitting procedure (approximately equal to η_o). Table 3 lists the values used. Figure 2 plots the tissue attenuation as a function of thermal dose. It was assumed that the ultrasonic absorption was 90% of the value of attenuation (Gertner et al. 1997) throughout the entire temperature range. Hence, any reference to changes into attenuation imply a corresponding change in tissue absorption.

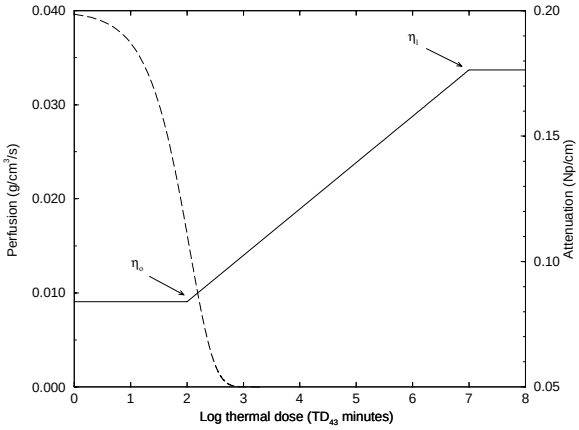

Figure 2. *Plot of perfusion (dotted line, left axis) and attenuation (solid line, right axis) as a function of thermal dose according to equation 4. The attenuation starts increasing at a TD_{43} of 100 minutes and remains constant beyond 10^8 minutes. Note that no perfusion was assumed in the simulations presented however*

3 Results

The normalised free field intensity distribution of the calculated beam is shown in figure 3. The arrow joining the horizontal lines delineates the axial portion of the free-field focal region (the region enclosed by the 50% intensity contour). The area enclosed in the focal region is a good predictor of lesion size for short insonication times for lesions of thermal origin (Watkin et al. 1996).

Figure 4 plots predicted lesion dimensions for the irradiation of the *in-vitro* liver for both cases of no change in attenuation (line labelled "nc") and the attenuation changing as a function of thermal dose according to equation 4 (line labelled "x2.1"). The effects of changing attenuation on lesion location and size are small, increasing with intensity. These results are *in contrast* to the results reported by Watkin et al. (1996) for which the lesions formed in the liver were not centred about the free-field ultrasound focus.

Changes in the absorbed power distribution and temperature profiles due to anticipated increase in attenuation (by a factor of 2.1) are demonstrated in figure 5. The attenuation increase results in increased power deposited in the tissue which causes a substantial temperature increase at the focus compared to the case of constant attenuation. However, lesion size does not change appreciably and a slight (2 mm) shift of the lesion axial midpoint occurs.

If the factor by which the attenuation increases is modified in equation 4 from 2.1 to 5,10 or 20 while maintaining the same thermal dose thresholds, there is a substantial change in the lesion shape and dimensions (figure 6). An attenuation increase of this magnitude would be due to non-thermal mechanisms of enhanced power deposition such as bubble formation and cavitation. The general shape of the thermal dose isocontours shifts from the typical "cigar shape" lesion to more of a "carrot shape". Although such lesion characteristics closely match those seen experimentally, the change in axial location of the lesion front does not match that recorded in the experiments of Watkin et al. (1996); the experimental lesion front is located close to the surface of the tissue/waterbath interface (corresponding to the axial location of 3 cm in figure 6).

[2]the code can be downloaded from the U.R.L. http://www.netlib.org

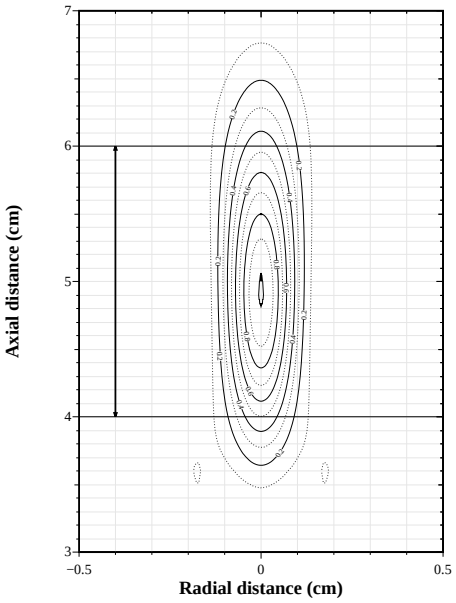

Figure 3. *Normalised intensity pattern contours for the transducer used in the simulations (10% contour lines). The arrow joining the horizontal lines represents the axial extent of the focal region.*

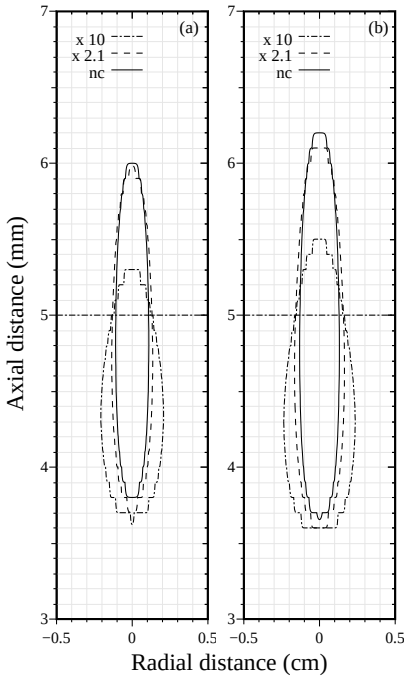

Figure 4. *Lesion contours calculated for the liver irradiations with overlying structures as described in the main text for a) I_{sp} 3430 W/cm^2 ($\eta_l \times$ 1, 2.1 and 10 η_o) and b) I_{sp} 4660 W/cm^2 ($\eta_l \times$ 1, 2.1 and 10 η_o). Horizontal lines represent focal depth.*

4 Discussion

For the lower intensities used in this work, there is a general agreement between experiment and theory in terms of lesion size close to the focus. However, for higher intensities there are disparities. The theoretical model did not predict that in the *in-vitro* liver experiments the lesion boundary would extend beyond the axial location of 136 mm. In the experiments and for the intensity of 4200 W/cm^2 however the lesion front extended to 124 mm. It is clear from the experimental data that either a non-thermal source is the causative agent of the visible lesion or the power deposition pattern is modified such that it significantly migrates towards the transducer. The power deposition pattern can be modified by any factors that would influence the terms in equation 3.

Dynamic property changes in ultrasonic attenuation due to tissue coagulation affect lesion formation, even for the short 2 second exposure time used in these simulations. Figure 5 demonstrates the temperature profiles predicted with and without accounting for dynamic changes in the attenuation and absorption coefficient as a function of thermal dose. While the actual lesion shape does not change significantly (figure 4), the increase in the power absorbed and temperature at the focus is substantial. In figure 5 the maximum temperature reached surpasses the boiling point at which vapour may be formed in the tissue leading to bubble formation. Furthermore, high temperatures reduce the tissue cavitation threshold levels (Frizzell 1988; ter Haar 1988). Therefore, the higher temperatures would favour the formation of bubbles due to tissue boiling and would concurrently reduce the tissue cavitation threshold levels.

Non-thermal damage can be caused by cavitation within the tissue or in the watertank close to the tissue surface. Cavitation refers to the process by which gas-filled or vapour-filled cavities (bubbles) are formed in a medium exposed to an ultrasonic field (ter Haar 1988). Such cavities would scatter ultrasonic energy efficiently, enhancing tissue absorption in their near vicinity and redirecting the ultrasound beam. Furthermore, if many such cavities form they can act as a propagation barrier, reducing the power deposited in the tissue beyond that barrier. Cavitation most likely occurred in some of the experiments modeled since the intensities used were greater than published cavitation thresholds. Meanwhile, the cavitation threshold increases with frequency and decreases with increasing gas content and temper-

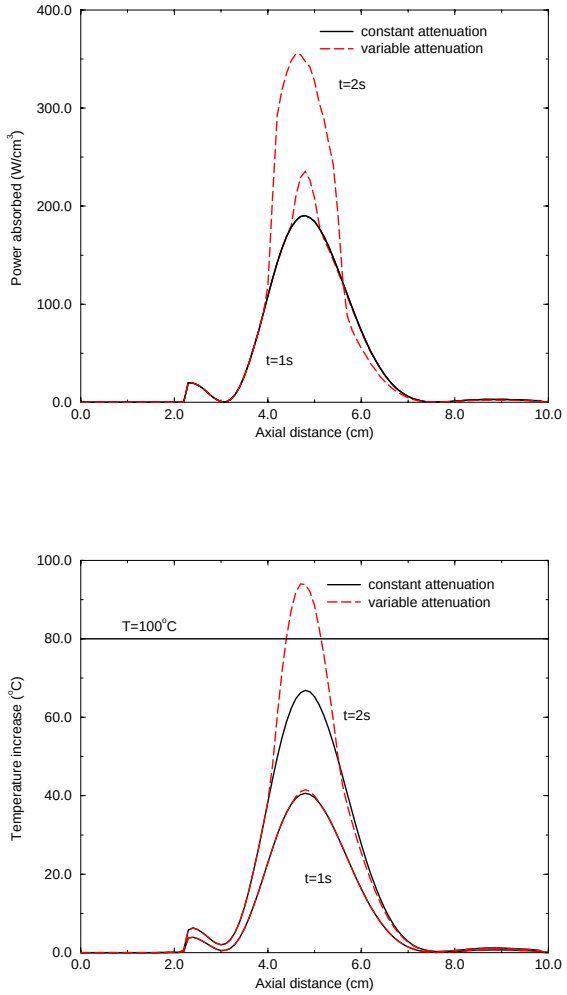

Figure 5. *Changes in a) the axial power absorbed and b) the axial temperature profiles during the first and second seconds of the HIFU exposure (I_{sp}=1220 W/cm^2) without (solid line) and with (dashed line) taking into account changes in the liver attenuation. Horizontal line in a) represents the 100°C mark (assumed point at which tissue boils).*

ature. Therefore cavitation is more likely to occur in hot regions of the treatment field, especially in regions where the temperature exceeds 100 °C. This likely triggers a positive feedback loop in which the increased attenuation/absorption creates higher temperatures, more vapour, and thus cavitation nuclei.

The high absorption coefficients used in a subset of the simulations ranging from a factor of 5 to 20 greater than the non-lesioned attenuation value (figures 6) can be thought to model the

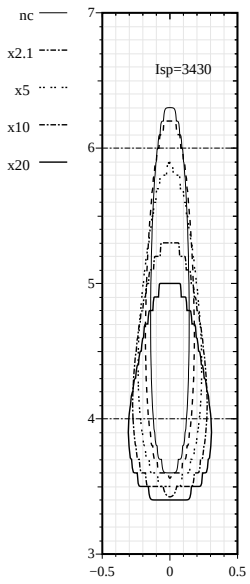

Figure 6. *Changes in lesion shape and for t=2s irradiations (I_{sp}=3430 W/cm^2) in which the change in attenuation coefficient from non-lesioned to lesioned tissue varies from 2.1 to 20.*

situation in which accumulation of vapour and bubbles would locally increase the attenuation coefficient. The theoretical model in this case predicts some of the trends observed in the experiments of Watkin et al. (1996): the increase in lesion width proximal to the transducer, the migration (up to a certain point) of the lesion front towards the transducer and the decrease of the maximum observed lesion depth. The overall result is a lesion the resembles a “carrot” more than the traditional “cigar”.

The effect of bubble formation has been modeled as an increase in the attenuation coefficient of the irradiated tissue that follows the kinetics of tissue coagulation. The kinetics and thresholds for bubble formation will undoubtedly be different from those that govern tissue coagulation. However for the short irradiations times used it can be thought as a first approximation.

Another interesting point is that the lesion threshold for tissue necrosis *in-vivo* and for tissue whitening *in-vitro* substantially differ (table 3). This is because the endpoints are different: in the one instance cell viability is assessed and in the other visible changes of a biochemical process which would require higher temperatures and longer exposures. Notably, the threshold TD_{43} used to model tissue whitening derived by matching the experi-

mental ox liver and theoretical lesion width at the focus is similar to the thermal dose at which the change in attenuation plateaus in dog liver (figure 2).

5 Conclusions

Changes in tissue ultrasonic attenuation and absorption during HIFU irradiation of tissues are predicted to play an important role in lesion creation if the intensities used are sufficient to produce non-thermal effects. It is shown that if changes in attenuation due to lesion formation are not taken into account, then the temperatures predicted by thermal models underestimate the tissue temperatures thus potentially missing undesirable effects such as tissue boiling and cavitation. Using the anticipated change in attenuation due to tissue coagulation, the predicted lesions did not match qualitatively or quantitatively the experimental lesions produced by Watkin et al. (1996) for high intensities. However, when increasing the attenuation up to twenty-fold in the lesioned tissue to mimic enhanced attenuation due to bubble formation, the lesions qualitatively match the mentioned lesions. It was concluded that if all the tissue damage was of thermal origin, then the tissue attenuation must have increased by a factor of 10-20 to match the predicted and measured lesion shapes qualitatively.

REFERENCES

Arditi, M., F. S. Foster, and J. W. Hunt (1981). Transient fields of concave annular arrays. *Ultrasonic Imaging 3*(1), 37–61.

Borelli, J., L. L. Thompson, C. C. Cain, and W. C. Dewey (1990). Time-temperature analysis of cell killing of BHK cells heated at temperatures in the range of 43.5 C to 57.0 C. *International Journal of Radiation Oncology, Biology and Physics 19*, 389–399.

Burgess, S. E., R. H. Silverman, D. J. Coleman, M. E. Yablonski, F. L. Lizzi, J. Driller, and A. R. and (1986, June). Treatment of glaucoma with high-intensity focused ultrasound. *Ophthalmology 93*(6), 831–8.

Damianou, C. A., K. Hynynen, and X. Fan (1995). Evalution of accuracy of a theoretical model for predicting the necrosed tissue volume during focused ultrasound surgery. *IEEE Transactions on Ultrasonics, Ferroelectrics and Frequency Control 42*(2), 182–187.

Damianou, C. A., N. T. Sanghvi, F. J. Fry, and R. Maass-Moreno (1997). Dependence of ultrasonic attenuation and absorption in dog soft tissues on temperature and thermal dose. *Journal of the Acoustical Society of America 102*(1), 628–634.

Frizzell, L. A. (1988). *Ultrasound : its chemical, physical, and biological effects*, Chapter Biological Effects of Acoustic Cavitation, pp. 287–304. New York, N. Y.: VCH Publishers.

Fry, W. J. and F. J. Fry (1960). Fundamental neurological research and human neurosurgery using intense ultrasound. *IRE Transactions in Medical Electronics ME-7*, 166–181.

Gertner, M. R., B. C. Wilson, and M. D. Sherar (1997). Ultrasound properties of liver tissue during heating. *Ultrasound in Medicine and Biology 23*(9), 1395–1403.

Gertner, M. R., A. E. Worthington, B. C. Wilson, and M. D. Sherar (1998). Ultrasound imaging of thermal therapy in ex vivo liver. *Ultrasound in Medicine and Biology 24*(7), 1023–32.

Kolios, M. C., M. D. Sherar, and J. W. Hunt (1995). Large vessel cooling in heated tissues: A numerical study. *Physics in Medicine and Biology 40*(4), 477–494.

Kolios, M. C., M. D. Sherar, and J. W. Hunt (1996). Blood flow cooling and ultrasonic lesion formation. *Medical Physics 23*(7), 1287–1298.

Linke, C. A., W. Lounsberry, and V. Goldschmidt (1967). Localized heating of tissue by electric and nonelectric means. *Investigative Urology 4*(6), 586–599.

Malcolm, A. L. and G. R. ter Haar (1996). Ablation of tissue volumes using high intensity focused ultrasound. *Ultrasound in Medicine & Biology 22*(5), 659–669.

Patankar, S. V. (1980). *Numerical heat transfer and fluid flow*. Washington, D. C.: Hemisphere.

Sanghvi, N. T., F. J. Fry, R. Bihrle, R. S. Foster, M. H. Phillips, J. Syrus, A. V. Zaitsev, and C. W. Hennige (1996). Noninvasive surgery of prostate tissue by high-intensity focused ultrasound. *IEEE Transactions on Ultrasonics, Ferroelectrics and Frequency Control 43*(6), 1099–1110.

Sapareto, S. A. and W. C. Dewey (1984). Thermal dose determination in cancer therapy. *International Journal of Radiation Oncology, Biology and Physics 10*, 787–800.

ter Haar, G. R. (1988). *Ultrasound : its chemical, physical, and biological effects*, Chapter Biological Effects of Ultrasound in Clinical Applications, pp. 305–319. New York, N. Y.: VCH Publishers.

Vallancien, G., M. Harouni, B. Guillonneau, B. Veillon, and B. J. (1996). Ablation of superficial bladder tumors with focused extracorporeal pyrotherapy. *Urology 47*(2), 204–207.

Watkin, N. A., S. B. Morris, I. H. Rivens, C. R. Woodhouse, and G. R. ter Haar (1996). A feasibility study for the noninvasive treatment of superficial bladder tumours with focused ultrasound. *British Journal of Urology 78*(5), 715–721.

Watkin, N. A., G. A. ter Haar, and I. Rivens (1996). The intensity dependence of the site of maximal energy deposition in focused ultrasound surgery. *Ultrasound in Medicine & Biology 22*(4), 483–91.